RESEARCH ARTICLE

Hourly remote sensing monitoring of harmful algal blooms (HABs) in Taihu Lake based on GOCI images

Hongye Cao[1] · Ling Han[2]

Abstract

The increasingly serious harmful algal blooms (HABs) in Taihu Lake has brought huge losses to the local economy and people's life in Taihu Lake. Satellite remote sensing technology has become one of the most important monitoring methods for HAB disasters due to its large-scale and long-term advantages. GOCI image has become the new data source of HAB monitoring because of its large size and high time resolution. Due to the low spatial resolution (500 m) and the existence of mixed pixels, the error of HAB area obtained by the NDVI method is large. In this paper, the linear mixing model (LMM) and the normalized difference vegetation index (NDVI) threshold method are combined to extract the HAB area from GOCI images with 500-m spatial resolution. Compared with the results of the HAB area extracted by Landsat8 OLI and MODIS data, three small areas in the study area were selected to verify the accuracy of the HAB area extracted from the GOCI image on October 2, 2015. The results show that when the NDVI threshold is 0.1, the area error of HABs is the smallest when the extracted HAB pixels mask the decomposition results of mixed pixels; besides, the area error of HABs extracted from the GOCI image is smaller than that from MODIS image; finally, GOCI image can extract the spatial dynamic distribution of HABs in Taihu Lake within 8 h a day, which has higher temporal resolution than the MODIS image. Compared with the NDVI threshold method and LMM method, the inversion accuracy is greatly improved, and the accuracy is stable in different regions. It can provide technical support for the decision-making and assessment of HAB ecological disasters.

Keywords GOCI · MODIS · HABs · Taihu Lake · NDVI · LMM

Introduction

For a long time, it has been the case that eutrophication of lakes is a common environmental problem faced by freshwater lakes in China (Jiang et al. 2015; Luo et al. 2016). HAB is an ecological phenomenon in which algae proliferate in eutrophication freshwater lakes under certain environmental conditions and float on the water surface to cause abnormal watercolor (Huisman et al. 2005; Liu and Yang 2012; Qin et al. 2016). The main HABs in inland waters are cyanobacteria (Pal et al. 2020). The research demonstrates that many cyanobacteria are toxic (Chorus and Bartram 1999). The outbreak of cyanobacteria will not only affect the safety of drinking water supply (Guo 2007; Qin et al. 2010) but also lead to the disruption of the water food chain (Diaz and Rosenberg 2008), and the anaerobic water will affect aquatic organisms (Micheli 1999) and may eventually lead to a decline in water biodiversity (Vonlanthen et al. 2012). Consequently, to eliminate the adverse effects of HABs on the ecological environment and social stability, it is very important to study the temporal and spatial distribution of HABs (Kwon et al. 2020).

To effectively control the HABs in Taihu Lake, we must have a clear understanding of the whole process of its occurrence, development, and extinction. The occurrence of HABs in Taihu Lake is marked by large outbreak areas and dramatic changes in time and space, while remote sensing is marked by a large-scale, rapid, continuous, dynamic, visible, and large amount of information (Nazeer et al. 2017). The identification of HABs in inland lakes based on remote sensing technology can better reflect the temporal and spatial differences and changes of HABs. Many researchers have carried out the

---

✉ Ling Han
hanl2019@126.com

1 College of Geological Engineering and Geomatics, Chang'an University, Xi'an, China

2 School of Land Engineering, Chang'an University, Xi'an 710064, China

monitoring methods of HABs using EOS/MODIS (Moderate Resolution Imaging Spectroradiometer from Earth Observing System), FY3, Landsat TM (Thematic Mapper), and other satellite data and achieved some research results (Cannizzaro et al. 2019; Li et al. 2005; Ma et al. 2009; Xu et al. 2008; Zhou et al. 2008); some scholars have used MODIS satellite data to monitor the HABs in Taihu Lake (Yang et al. 2016); some scholars have used a multi-source satellite data (MODIS, Landsat TM, etc.) to analyze the temporal and spatial distribution of HABs in Taihu Lake (Duan et al. 2012; Duan et al. 2008; Ma et al. 2008; Qi et al. 2014). However, the occurrence of HABs is affected by many factors, such as water quality environment and meteorological conditions, which lead to its rapid development and change (Wang et al. 2020; Wang et al., 2019 b). Conventional remote sensing images cannot meet the needs of dynamic monitoring of HABs in terms of timeliness and dynamic tracking (Hu et al. 2019; Lei et al. 2020).

GOCI is a sensor on Communication, Ocean, and Meteorological Satellite (COMS), the first stationary sea color satellite launched by South Korea in 2010 (Higa et al. 2020; Tang et al. 2019). It can observe the ocean and coastal waters with the spatial resolution of 500 m and the time resolution of updating once an hour and eight times per day (Hu et al. 2019). It has the characteristics of high spatial coverage and high temporal resolution. While recognizing the HABs, it can discover the spatial dynamic change of the HABs in time and study its dynamic migration process in the lake (Noh et al. 2018). It has important practical significance for monitoring and early warning of the HABs in Taihu Lake.

In the near-infrared band, HABs have a high reflectance, while the near-infrared band is a strong absorption band of water. Near-infrared data can clearly distinguish HABs and lake water (Gu et al. 2011), which makes it possible to extract HAB information with high precision by using a mixed pixel decomposition method. The main decomposition models of mixed pixels include the linear mixed spectral model, the fuzzy supervised classification model, and the neural network model (Lv et al. 2003). The most commonly used model of mixed pixel decomposition is the linear mixed model (LMM). The LMM method combined with the NDVI threshold method to extract HABs from GOCI images has not been reported.

To address this knowledge gap, in this study, GOCI images are selected to extract HABs by LMM-NDVI, with Taihu Lake as an example. Based on the region of HABs extracted by NDVI, the mixed pixels are decomposed by LMM, and the results are cross-validated with high spatial resolution images (Landsat8 OLI). The hourly distribution of HABs in Taihu Lake was extracted by GOCI images, and the dynamic change was analyzed with meteorological data. Therefore, the purpose of this study is (1) to evaluate the application of LMM-NDVI in the extraction of HAB area, (2) to evaluate whether GOCI image can be used to monitor HABs in Taihu Lake, and (3) to emphasize the importance of high-frequency

observation for environmental management and planktonic algae research.

Materials and methods

Study area

Taihu Lake (30°55′40″~31°32′58″N, 119°5232″~120°36′10″ E) is the third largest fresh water lake with an area of 2428 km^2 (water surface area is 2338 km^2; island area is 90 km^2) and a mean depth of 1.9 m in China (Xue et al. 2020; Yao et al. 2020). Taihu Lake plays an important role in basin irrigation and urban and rural water supply (Xie et al. 2020). In the recent 20 years, with the rapid development of industrial and agricultural production, the eutrophication of Taihu Lake water is serious, and large-scale HABs will break out every year (Luo et al. 2020). It is worth noting that the eastern coastal area of Taihu Lake is clear, with a large number of aquatic vegetation growth, which greatly interferes with the extraction of HABs, which is not involved in this study (dark gray part in Fig.1) (Fu et al. 2015).

Data acquisition and processing

COMS GOCI image processing

GOCI level 1B satellite image data were obtained from the Korea Ocean Satellite Center (http://kosc.kiost.ac/eng/). GOCI data has 8 bands (Table 1), with a spatial resolution of 500 m and a time resolution of 1 h. It can provide 8 images between 8:30 and 15:30 Beijing time every day (Yeom et al. 2015). This study requires pre-processing of GOCI remote sensing image data, including radiometric calibration, geometric correction, atmospheric correction, and extraction of water bodies in the study area.

The geometric correction of GOCI images is done by GLT geometric correction method (Wang et al. 2018). The GOCI images are radiometrically corrected using radiometric calibration parameters and formulas (Du et al. 2017). GOCI image is a relatively new remote sensing data, and there is less research on it at home and abroad, and there is no mature atmospheric correction algorithm (Du et al. 2017). The latest GOCI data processing software GDPS VII on the official website provides the atmospheric correction algorithm (Ahn et al. 2012). However, the algorithm is applicable to coastal waters, and the applicability to two inland water bodies needs further validation. The 6S atmospheric correction method is one of the commonly used atmospheric correction methods for remotely sensed images of terrestrial water bodies and has been adopted in later studies (Huang et al. 2015). And then, we used the 6S (Second Simulation of Satellite Signal in the Solar Spectrum) method to eliminate the aerosol and other

Fig. 1 Location of Taihu Lake within China and subarea of Taihu Lake. The red triangle represents the Taihu Lake Meteorological Station (Dongshan meteorological station)
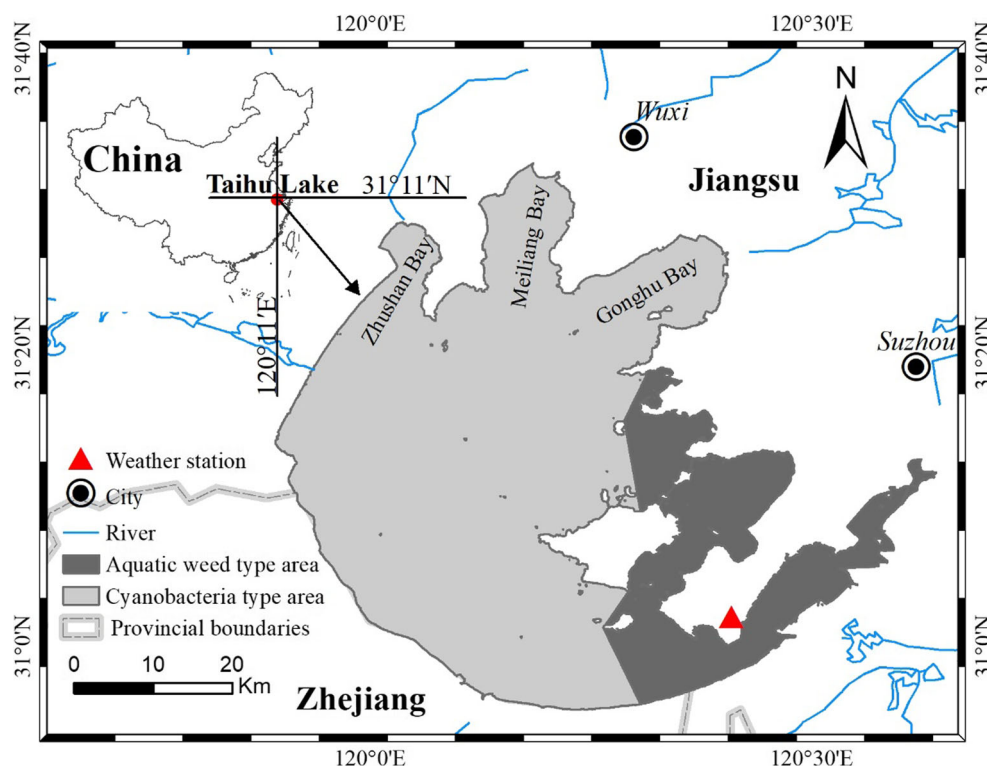
atmospheric effects and then realized the atmospheric correction of GOCI data (Pang et al. 2018; Yeom et al. 2020).

Other image processions

This study was validated using MODIS L1B data (https://ladsweb.modaps.eosdis.nasa.gov/) synchronized with GOCI. The MODIS L1B data were reprojected using the MODIS Conversion Toolkit (MCTK) (Universal Transverse Mercator). Then, the atmospheric correction of MODIS is

completed by 6S atmospheric correction method, and real surface reflectance data is obtained (Ma et al. 2016).

Landsat8 OLI is a solar synchronous orbit satellite, with a spatial resolution of 30 m and an orbit height of 705 km(Yu et al. 2016). Radiation correction and atmospheric correction based on the 6S radiation transmission model were performed on the Landsat8 OLI image in turn, and finally, the reflectance image of the study area was obtained (Bonansea et al. 2015; Wang et al. 2019a).

Table 1 Technical specification for GOCI, MODIS, and Landsat8 OLI in the VIS-SWIR bands[a]

GOCI				MODIS				Landsat8 OLI			
WL (nm)	BW (nm)	SR (m)	SNR	WL (nm)	BW (nm)	SR (m)	SNR	WL (nm)	BW (nm)	SR (m)	SNR
412	20	500	1000	412.5	15	1000	880	440	20	30	130
443	20	500	1190	443	10	1000	8380	480	60	30	130
490	20	500	1170	488	10	1000	802	560	60	30	100
555	20	500	1070	531	10	1000	754	655	30	30	90
660	20	500	1010	550.5	11	1000	750	865	30	30	90
680	10	500	870	667	10	1000	910	1610	80	30	100
745	20	500	860	678	10	1000	1087	2200	80	30	100
865	40	500	750	748	10	1000	586	-	-	-	-
-	-	-	-	869.5	15	1000	576	-	-	-	-

[a] Source of GOCI specifications, KOSC (https://kosc.kiost.ac.kr/eng/); MODIS specifications, NASA (https://oceancolor.gsfc.nasa.gov/); and Landsat8 OLI specifications, USGS (https://earthexplorer.usgs.gov/). WL, BW, SR, and SNR represent wavelength, bandwidth, spatial resolution, and signal noise ratio, respectively.

Method

NDVI

NDVI is a vegetation index method with a better application effect (Cao et al. 2018; Cho and Ramoelo 2019). Because the spectral characteristics of the HABs are similar to those of vegetation, the information of HABs can be extracted effectively according to NDVI (Oyama et al. 2015; Shi et al. 2019). NDVI is defined as the normalized ratio of the red band and the near-infrared band (Norris and Walker 2020), namely:

$$NDVI = \frac{Rrs(NIR) - Rrs(Red)}{Rrs(NIR) + Rrs(Red)} \quad (1)$$

where $Rrs(NIR)$ and $Rrs(Red)$ represent the reflectance of the near-infrared band and red band, respectively, for the MODIS image; they represent the reflectance of band 9 (869.5 nm) and band 6 (667 nm), respectively; for the GOCI image, they represent the reflectance of band 8 (865 nm) and band 5 (660 nm), respectively; and for the Landsat8 OLI image, they represent the reflectance of band 5 (865 nm) and band 4 (655 nm), respectively (Table 1).

According to the band settings of GOCI, MODIS, and Landsat8 OLI, the information of HABs is extracted by the threshold method using the NDVI model, and the discriminant equation is as follows:

$$NDVI > NDVI_t \quad (2)$$

In Eq. 2, $NDVI_t$ represents the threshold value of NDVI. To ensure the accuracy of the HABs, the threshold value is determined by human–computer interaction. When the NDVI value is greater than the threshold value, the pixels are considered as HAB pixels.

LMM method

LMM is a common method of mixed pixel decomposition, which is defined like that in the image after atmospheric correction; the reflectance of a pixel in a certain band is a linear combination of the endmember (pixel containing only one kind of feature information) reflectance of the component pixel with the proportion of its pixel area as the weight coefficient (Lyit and Genc 2011). The mathematical expression of LMM is as follows (Kim et al. 2020; Meng et al. 2007):

$$R_{i\lambda} = \sum_{k=1}^{n} f_{k\lambda} \cdot C_{k\lambda} + \varepsilon_{i\lambda} \quad (3)$$

$$\sum_{k=1}^{n} f_{k\lambda} = 1 \quad (4)$$

where $R_{i\lambda}$ is the reflectance of the i-th pixel in the λ band (known); f_{ki} is the ratio (to be determined) of the area of the k-

th endmember ($k = 1, 2, …, n$) corresponding to the i-th pixel; $C_{k\lambda}$ is the spectral reflectance of the k-th basic component in the λ band; $\varepsilon_{i\lambda}$ is the residual error; and n is the number of basic components (the main purpose of this study is to distinguish lake water and HABs, so the value here is 2), and the number of available bands in the mode should be greater than n, to solve the problem by the least square method.

LMM separates $R_{i\lambda}$ from the mixed pixels and extracts the average reflectance $C_{k\lambda}$ of each endmember. By solving the linear equation, the area ratio f_{ki} of the endmember in the pixel is inversely solved, so that all the pixels are decomposed into the components of these basic components. The results of LMM calculation are the magnitude image of each endmember and the residual error image. Generally, the residual error should be as small as possible, and the component f after pixel decomposition should meet the standard of $0 \leq f \leq 1$ to evaluate the quality of endmember selection.

Pure pixel selection

The correct selection of pure water and bloom pixels is the key to the successful implementation of the linear decomposition method. The pixels in the whole lake area can be simplified into three regions: pure water body pixels, pure HAB pixels, and mixed pixels of water and HABs. The specific methods for the selection of the two types of pure pixels are as follows: The HAB area is selected by visual judgment, and the pixel with the highest NDVI value is selected as the HAB pixel; in the lake area, the pixel with the lowest DN value or the sum of reflectance values is selected as the pure water pixel (10 minimum pixels can be selected for the average in specific operation).

Area of HABs based on LMM-NDVI

Due to the presence of mixed pixels, there may be some HAB information in non-HAB pixels in low spatial resolution images, which has certain errors in the calculation of the HAB area. The steps of extracting HABs based on the LMM-NDVI method are as follows: first, the NDVI threshold method is used to extract the pixels of the HABs of the GOCI image; then, the HAB pixels are used to mask the image that uses the LMM method to decompose the mixed pixels. The HAB area was obtained according to the masked HAB abundance value of the pixel (the percentage of HABs in the pixel).

Accuracy evaluation

The results of high spatial resolution images were used in some studies to validate that of low-resolution images (Ma et al. 2020). The area of HABs was extracted from the Landsat8 OLI images by the NDVI thresholding method (Eqs. 1 and 2) and used as the "true value" to evaluate the

results of the GOCI images. The area extracted from the MODIS image were used for parallel verification with GOCI. When extracting HABs from MODIS and GOCI images, the HAB pixels extracted by different NDVI thresholds will affect the calculation results of the HAB area. To find the most suitable NDVI segmentation threshold, this paper applies 8 thresholds 0.2, 0.15, 0.1, 0.05, 0, −0.05, −0.1, and −0.15 to extract HAB pixels. The results of HABs extracted by Landsat8 OLI were evaluated to obtain the most suitable NDVI threshold of HAB pixel segmentation. At the same time, considering the regional accuracy of different regions under different threshold conditions may be different. Three regions (red boxes in Fig. 2) were selected for evaluation on the GOCI image on May 27, 2015, and the NDVI thresholds of HABs in different regions were obtained.

Results

Cross-validation of GOCI-Rrs with MODIS and Landsat8 OLI

To evaluate the quality of GOCI image atmospheric correction, the method of cross-comparison of multiple satellites is widely used (Chen et al. 2019). In this paper, the results of GOCI atmospheric correction are compared with those of MODIS and Landsat8 OLI. The reflectance of GOCI, MODIS, and Landsat8 OLI was collected on October 2 and May 27, 2015. The area is located in the inner part of Taihu Lake (land pixels are excluded). Because the water body of East Taihu Lake is shallow and mainly aquatic plants, the area of East Taihu Lake is excluded in this paper (Fig. 1). Please

Fig. 2 Three small areas containing HABs selected on the GOCI image on May 27, 2015

take notice that the evaluation excludes 412-, 680-, and 745-nm bands of GOCI image, because MODIS and Landsat8 OLI data do not have the corresponding band. Among the four pairs of bands (490 vs 490 nm, 555 vs 550.5 nm, 660 vs 667 nm, 865 vs 869.5 nm) between GOCI-Rrs and MODIS-Rrs (Fig. 3), the highest matching degree is 490 vs 488 nm (R = 0.9034, RMSE (root mean square error) = 0.126, MRE (mean relative error) = 10.56%). For the other three bands, the relative error is lower than 15%, and the coefficient of determination is higher than 0.85. Therefore, the reflectance of the four bands of the two sensors after atmospheric correction is highly matched.

For five pairs of bands (443 vs 440 nm, 490 vs 480 nm, 555 vs 560 nm, 660 vs 655 nm, 865 vs 865 nm) between GOCI and Landsat8 OLI, the determination coefficients of four bands (except for the blue band) are high, the range is 0.86–0.93, and the RMSE value range is 0.083–0.137; MRE is less than 20% in these bands (Fig. 3). Therefore, the reflectance of the four bands of the two sensors after atmospheric correction is highly matched.

These results provide a basis for further monitoring of HABs by using GOCI-Rrs. On the other hand, these results reflect the careful calibration of GOCI in this paper.

Area of HABs extracted by different methods

The areas of HABs extracted by the Landsat8 OLI were 413.76 km², 50.28 km², and 40.33km², respectively, which were taken as "true values" (Table 2). The area of HABs was extracted from MODIS and GOCI images by the NDVI method (NDVI = 0.1), and the relative error of each area was calculated (Table 2). The area of three regions in MODIS and GOCI images was calculated, and the area error of each region was calculated (Table 2). The errors of the three regions (zone 1 and zone 2) extracted by the NDVI threshold method are relatively large (MODIS, 23.89~56.76%; GOCI, 18.65~39.35%), and the three regions extracted by the LMM method are also larger (MODIS, 20.75 ~ 41.25%; GOCI, 16.54~30.15%). It is not difficult to find that only the error of zone 3 is slightly small (the error of the extracting area with different methods of two kinds of images is maintained at about 20%).

The HAB area of the mixed pixel decomposition results after the mask was calculated. The error of the three regions was calculated based on the HAB area extracted by Landsat8 OLI (Table 3). In general, the error range of the three regions changed from negative to positive in the process of NDVI threshold change from 0.2 to −0.15. The error range of zone 1 is the largest (MODIS, −23.15~55.34%; GOCI, −20.91~41.56%), and the error of zone 3 is the smallest (MODIS, −10.98~13.56%; GOCI, −9.33~12.33%), and the error is slightly smaller. When NDVI is 0.1, the error of the three regions is the best. Besides, it is not difficult to find that
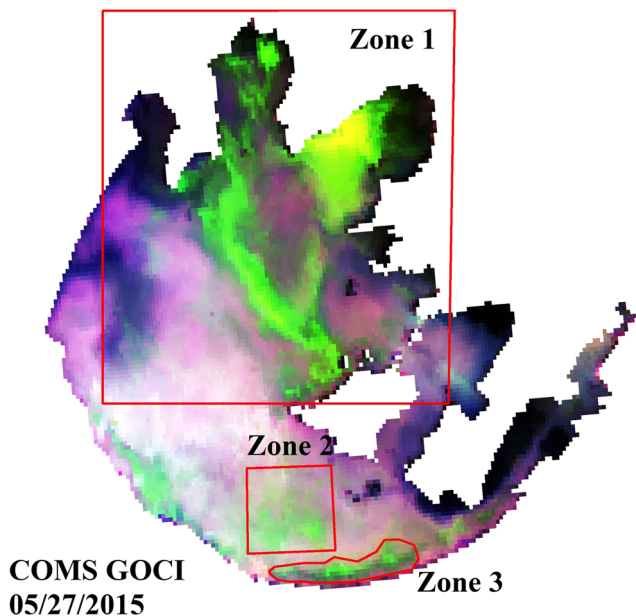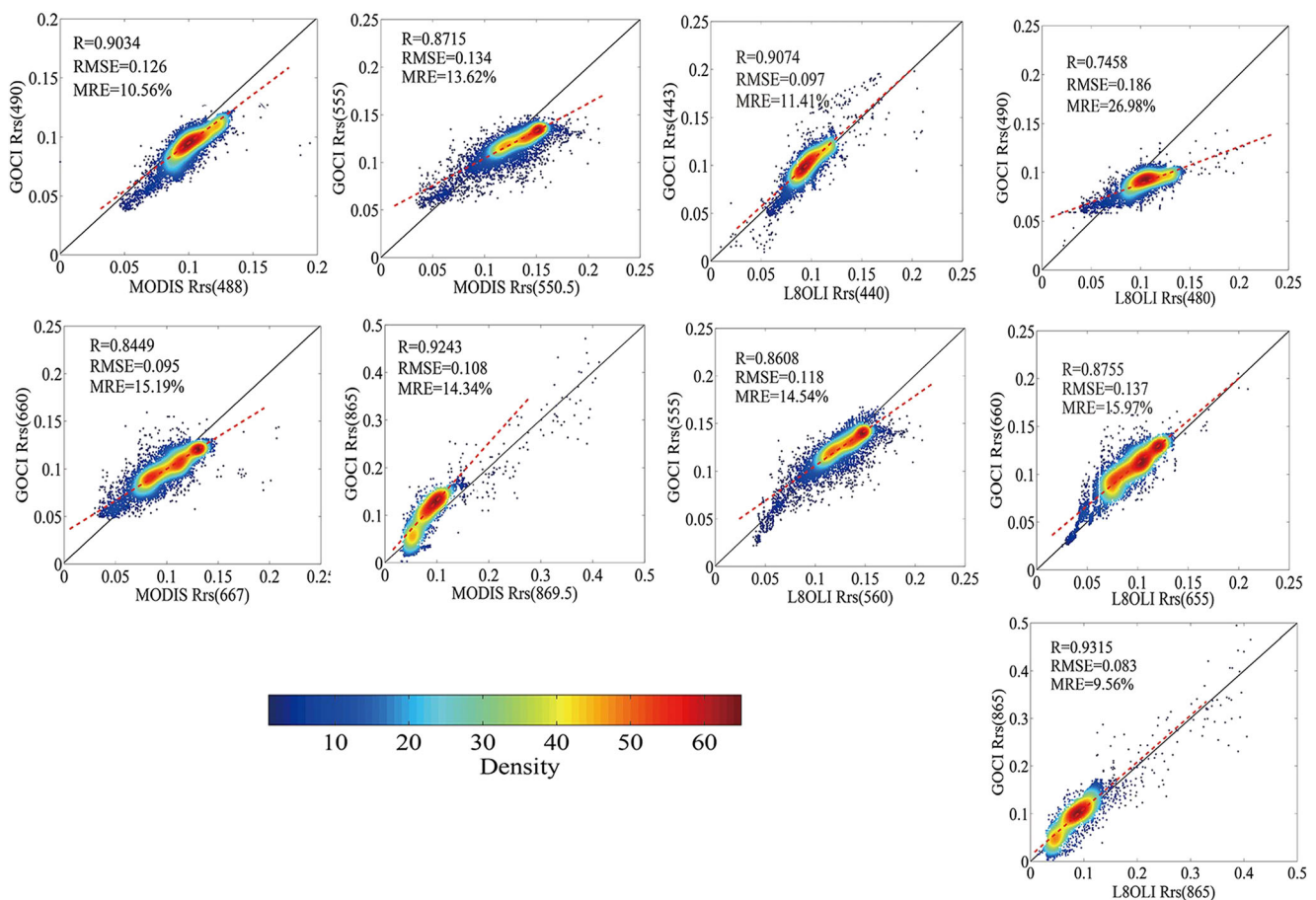
Fig. 3 Density scatter plot of comparison of GOCI-Rrs with MODIS-Rrs (upperside) and with Landsat8 OLI-Rrs (underside). The total number of matched points (*n*) is 31,965 for each pair. Three evaluation factors of R, RMSE, and MRE are marked in the scatter chart. The black oblique line is the 1:1 line, and the red oblique line is the regression line. In the figure, the dots of different colors represent the density, the dark blue represents the lowest density, and the red represents the highest density

the area error of the different regions of the GOCI image is lower than that of MODIS in the process of NDVI threshold change from 0.2 to −0.15.

Hourly dynamic analysis of HABs

As shown in Fig. 4, the hourly spatial distribution of HABs was extracted from the GOCI image on October 2, 2015, using the NDVI–LMM method. The hourly expansion and movement of algal patches are also detailed in the map (Fig. 5). At 8:16 on October 2, HABs first appeared in the northwest coastal area, the north coast of the north central area of the lake and Meiliang Bay, and the area of HABs was relatively small. Then, the HABs continued to expand from the northwest coastal area, the north of the lake center, and the Meiliang lake and reached the largest area at 10:16. Most of

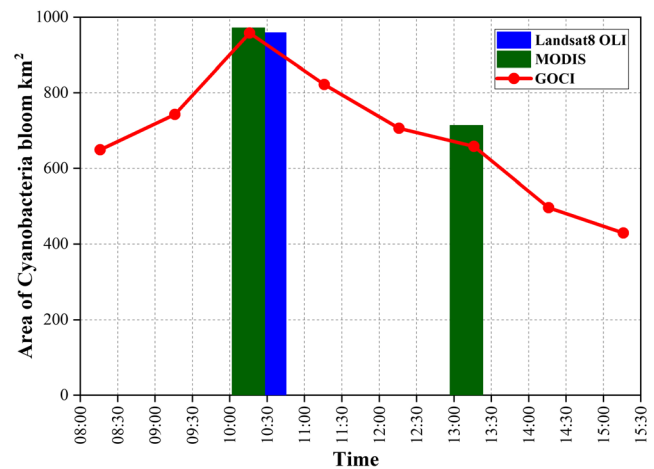**Table 2** The area error of different remote sensing images by NDVI and LMM method

Data	Method	Zone 1		Zone 2		Zone 3	
		Area (km²)	Error (%)	Area (km²)	Error (%)	Area (km²)	Error (%)
Landsat8 OLI	NDVI threshold method	413.76	-	50.28	-	40.33	-
MODIS	NDVI threshold method	648.61	56.76	74.98	49.12	49.96	23.89
MODIS	LMM	584.44	41.25	69.98	39.19	48.70	20.75
GOCI	NDVI threshold method	576.57	39.35	65.96	31.19	47.85	18.65
GOCI	LMM	538.51	30.15	59.73	18.79	47.00	16.54

Table 3 The area error (%) of HABs extracted by the NDVI–LMM method

NDVI threshold	MODIS			GOCI		
	Zone 1	Zone 2	Zone 3	Zone 1	Zone 2	Zone 3
0.2	−23.15	−25.76	−10.98	−20.91	−21.34	−9.33
0.15	−20.79	−19.76	−9.87	−12.33	−12.34	−8.65
0.1	−10.23	−9.76	5.43	−11.12	−7.04	7.11
0.05	11.98	10.12	11.87	8.98	14.33	10.88
0	25.87	29.76	13.45	22.78	20.65	9.34
−0.05	31.44	35.98	11.45	27.64	28.22	10.98
−0.1	40.25	42.34	10.98	31.25	32.26	10.45
−0.15	55.34	40.12	13.56	41.56	37.34	12.33

Fig. 5 Diurnal change of the area of HAB patches in Taihu Lake on October 2, 2015. Red dot and line, area derived from GOCI-NDVI; green bar, area derived from MODIS-NDVI; blue bar, area derived from Landsat8 OLI-NDVI

the shore in the northwest of Taihu Lake, the western waters in the north of the lake center, and most of the waters in Meiliang lake are covered by HABs while only a small amount of HABs in the coastal areas and the lake center in the southwest. The HABs decreased gradually from 11:16. There was only a small amount of HABs along the northern coast of the north part of the lake center at 15:16. Figure 5 intuitively shows the hourly change of HABs in Taihu Lake, that is, it first increases gradually to the peak value and then decreases gradually. MODIS image can only reflect the HAB area at 10:15 and 13:30. Not to mention Landsat8 OLI, it can only reflect the distribution of the peak area of HABs at 10:16.

For some cloudy images (June 12, 2018), it is difficult to understand the diurnal variation of HABs in the whole lake

due to the partial coverage of clouds (Fig. 6). It is not difficult to find that the HAB plaques in the northwest of Taihu Lake are visible, at least between 8:16 and 15:16. Besides, the daily dynamic changes of HAB patches can be roughly seen through GOCI images. From 8:16 to 11:16, the area of HAB patches increased gradually. From 12:16 to 15:16, the patch area of HABs decreased gradually. MODIS can only show that at 11:05 and 12:40, there may be HAB patches in the Northwest Lake, not to mention Landsat8 OLI, which can only find possible HAB patches at some time.

The spatial distribution of HABs in Taihu Lake can be identified in detail by using the GOCI image. Conventional

Fig. 4 Distribution of HABs in Taihu Lake on October 2, 2015, with the Landsat8 OLI image (left upper), the MODIS images (left lower), the GOCI images (right). The green patches represent cyanobacteria, and the blue patches represent lake water
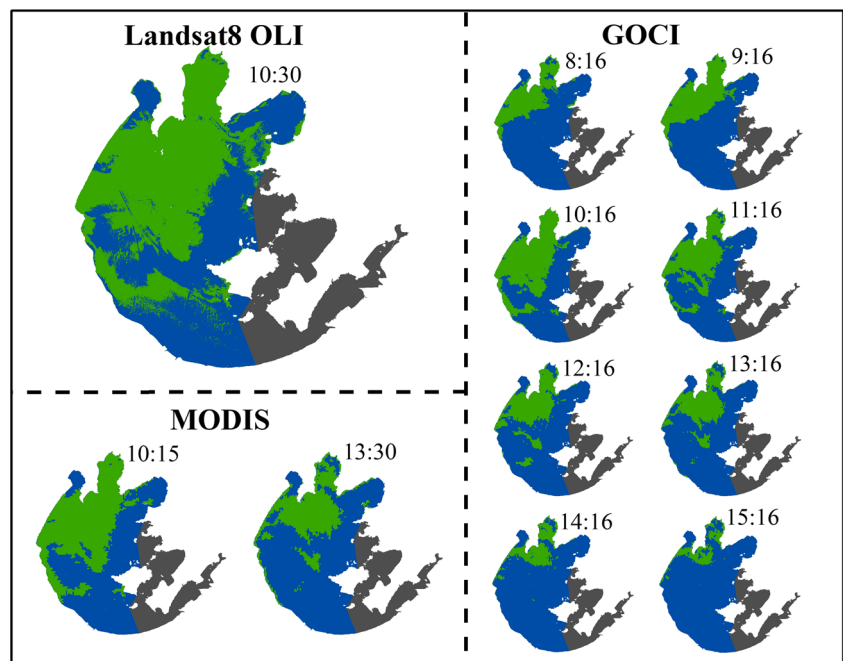
Fig. 6 Distribution of cyanobacterial bloom in Taihu Lake on June 12, 2018. Green, blue, and white patches represent cyanobacterial blooms, lake water, and cloud, respectively
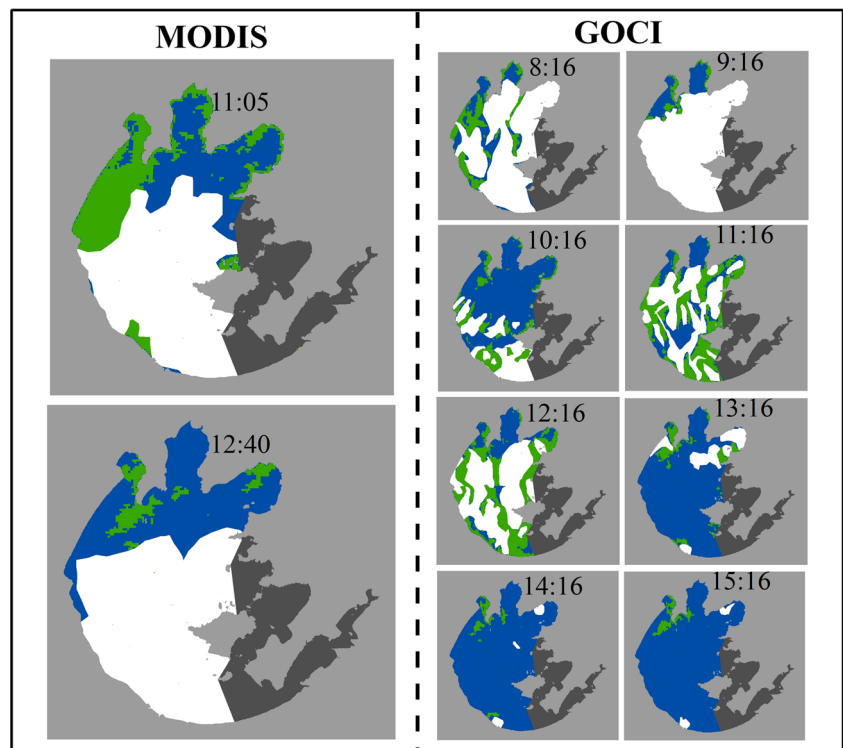
MODIS images only have one image in the morning and one in the afternoon, let alone Landsat8 OLI image in which its time resolution is 16 days.

Discussion

Error analysis of cross-validation of atmospheric correction

It is observed in Fig. 3 that the reflectance of the GOCI and Landsat8 OLI sensors after atmospheric correction has a high degree of matching (MRE < 20%, R > 0.85) except for the blue band. The matching degree of the four bands of the GOCI and MODIS two sensors is relatively high (MRE < 20%, R > 0.80). The difference in reflectance after atmospheric correction reflects the band characteristics (band center, etc.) of the three sensors and the difference in the observation geometry (Chen et al. 2019). Among them, there is a slight difference in the observation angle of the sensor (< 15° between GOCI and MODIS, < ~10° between GOCI and Landsat8 OLI). The blue band centers of the GOCI and Landsat8 OLI sensors differ by 10 nm (Table 1), but the difference in the centers of other bands is small (<5 nm), especially that the center wavelengths of the near-infrared bands of the GOCI and Landsat8 OLI sensors are equal. It can be found from Table 1 that the error here is the smallest (MRE = 9.56%, R = 0.9315, RMSE = 0.083). Therefore, the large error of the blue band after atmospheric correction of the GOCI and Landsat8 OLI sensors is

mainly caused by the large difference in the blue band center of the two sensors.

Error analysis of different extraction methods

The area extracted from MODIS and GOCI images using the NDVI threshold method is overestimated. The area of HABs extracted by the mixed pixel decomposition model is close to that extracted by Landsat8 OLI, but it is still overestimated. The reason for the overestimation of the area of the NDVI threshold method is that most of the pixels extracted by the NDVI threshold method are mixed pixels of HABs and water bodies. The calculated area includes the water area in the mixed pixel, so the area is much larger than the actual area. The reason why the area accuracy of the LMM model is higher than that of the NDVI threshold method is that the LMM model can retrieve the HAB abundance in the mixed pixels of HABs and water body, thus eliminating the interference of water body in the calculation of area. At the same time, it should be pointed out that even if the LMM method is used, the error is still very large, the error of zone 1 is more than 30%, the error of zone 1 is more than 20%, and only the error of zone 3 is relatively small (basically maintained at about 20%). This is because there are a large number of water body pixels in zone 1 and 2, and a certain amount of HAB information is reflected in the decomposition of mixed pixels, which has a great impact on area statistics. The error of zone 3 is the smallest because almost all the HAB pixels in zone 3 and the area error caused by water pixels can be ignored. It can

be seen that only using the LMM model to extract HAB area information cannot guarantee the accuracy, which is the reason why the LMM model and NDVI threshold method are combined to carry out the area inversion of HABs.

Generally speaking, the accuracy of the combined method of linear mixed model and NDVI threshold method is significantly higher than that of the NDVI threshold method or LMM only. This is because the non-HAB pixels are removed after the mask, so the area accuracy is improved. It can be seen that different NDVI threshold errors are different. During the NDVI threshold from −0.15 to 0.2, the HAB area changes from overestimation to underestimation. When the threshold value is −0.15, a large number of non-HAB pixels participate in the area calculation, which leads to the overestimation of the area. When the threshold value is 0.2, the area is underestimated, which indicates that the threshold value is too large, and some HAB pixels are eliminated, resulting in the area underestimated. When the threshold value is 0.1, the error of the three regions in MODIS and GOCI images is better than 15%; although the minimum error of each region cannot be guaranteed, the adaptability in different regions can be guaranteed. Therefore, the NDVI threshold of HAB pixel extraction can be taken as 0.1. At the same time, it can be found that the area error of zones 1 and 2 is greatly affected by the change of NDVI threshold, while the area error of zone 3 is very little affected by the change of NDVI threshold because most of the pixels in zone 3 are HAB pixels, and the influence of non-HAB pixels is small, so the area error fluctuates little with NDVI threshold change; while the area error of zones 1 and 2 are affected by NDVI threshold, the number of pixels involved in the area calculation varies greatly with the change of threshold value, so the error fluctuates greatly with the change of NDVI threshold.

Besides, it is not difficult to find from Table 4 that the area error of GOCI image extraction is always lower than that of MODIS image when the NDVI threshold method or LMM

Table 4 Daily change of the area and weather data of Taihu HABs based on GOCI on October 2, 2015[a]

Time	Area (km^2)	Wind speed (m/s)	Temperature (°C)
8:00	443.99	1.00	18.19
9:00	564.33	0.71	20.28
10:00	841.83	1.10	21.54
11:00	666.50	2.49	23.07
12:00	517.28	3.00	24.12
13:00	455.75	2.52	24.59
14:00	247.28	3.24	24.85
15:00	160.65	3.48	23.93

[a] Meteorological data comes from the China Meteorological Science Data (http://data.cma.cn/).

method is used to extract HAB area based on MODIS and GOCI images. This is because the spatial resolution of the MODIS image (1000m) is lower than that of GOCI (500 m) and the water bloom area in some mixed pixels is not included, so the extracted result is smaller than that of GOCI data.

Driving factors for the dynamic change of HABs

The occurrence of HABs is related to many factors, such as algae type, wind speed (Lips et al. 2003; Wu et al. 2013; Wu et al. 2012), wind direction, rainfall (Reichwaldt and Ghadouani 2011; Warren-Rhodes et al. 2007), the concentration of nitrogen and phosphorus nutrients (Foster et al. 2011; Glibert et al. 2004), light intensity (Wynne et al. 2010), temperature (Kong and Gao 2005), etc. The growth, drift, and upwelling of HABs in the specific lake area of Taihu Lake are mainly affected by meteorological conditions (Wang et al. 2019b). Besides, some studies have pointed out that different wind fields have a great influence on the horizontal and vertical distribution of algae in the lake, and there is a "critical wind speed," which ranges from 2 to 3 m/s. When the wind speed is less than the critical wind speed, the water surface can be approximately regarded as hydrodynamic calm, without wave and wave generation. On the surface of the water, algae rapidly drift to the windward bank along the wind direction with a large amount of accumulation; however, when the wind speed exceeds the critical wind speed, there will be wave action. The combination of wave, wind disturbance, and other factors will make the algae mix up and down in the water body, and the distribution is relatively uniform, so there will be no algae accumulation phenomenon, thus inhibiting the formation of HABs (Cao 2006).
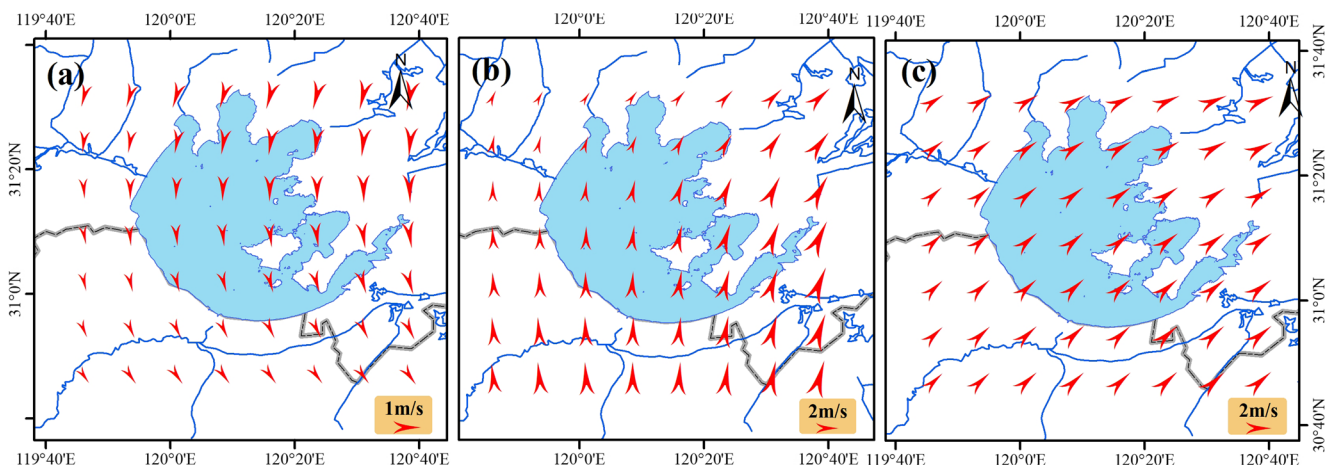
There is no precipitation and almost no difference in temperature on October 2, 2015 (Fig. 7 and Table 4), but the wind speed is quite different. The average wind speed is 1.4 m/s, far less than the critical wind speed, and the temperature is continuously high. A large number of cyanobacteria float to the northwest and form HABs.

As shown in Fig. 5, on October 2, HABs first appeared in the northwest and then gradually spread to the southeast from the northwest and Meiliang Bay. The average wind speed of the lake during 8:00–10:00 is 0.94 m/s, the maximum wind speed is not more than 2m/s, and the wind direction is mainly north wind (Table 4). Under the driving of wind, cyanobacteria float upward and gather to form HABs and drift to the downwind direction of the lake. With the rapid accumulation of algae, the HAB area reached the maximum at 10:00 (841.83 km^2). From 10:00, the area of HABs decreased gradually. The meteorological data show that the average wind speed from 12:00 to 15:00 is 3.06 m/s, and the maximum wind speed is 3.48 m/s, which exceeds the "critical wind speed." Compared with 8:00~10:00, the wind direction in this period changes, mainly southerly (Fig. 7). Under the influence

Fig. 7 Wind speed and direction over Taihu Lake on October 2, 2015: **a** 9:00, **b** 12:00, and (**c**) 15:00. Wind data were downloaded from ECMWF (European Centre for Medium-Range Weather Forecasts, https://www.ecmwf.int/)

of wind, the migration path of cyanobacteria changes and no longer spreads to the southeast. Due to the increase of instantaneous wind speed, the wind disturbance makes the algae mix up and down in the water body and no longer accumulate on the surface. Satellite monitoring shows that the area of HABs gradually decreases (Fig. 5, Table 4). It can be found that the wind directly drives the formation, movement, and disappearance of HABs. The results of the dynamic change of HABs and the analysis of wind speed and direction are consistent with the existing research results (Zhu and Cai 1997).

Potential application of GOCI images

GOCI image has a high time resolution (1 h), which is much higher than MODIS half-day time resolution (Chen et al. 2019). It makes it more likely to get clear images in some rainy and cloudy seasons. Because of this high sampling frequency, GOCI can reveal more details about the diurnal changes of HABs in Taihu Lake. Therefore, it is very necessary and meaningful to apply the satellite image to other coastal waters to provide important information about the floating algae, which can be used to help more inland and coastal waters for water environment monitoring and management.

On the other hand, the data of the GOCI satellite for sea color analysis consists of eight bands, which are 680- and 745-nm bands (red light absorption band of chlorophyll concentration) increased compared with SeaWiFS. It can be used for the inversion of chlorophyll in water and accurate correction of the atmosphere (Ahn et al. 2012). The waveband of the GOCI satellite is almost the same as that of MODIS, the most authoritative ocean color sensor at present (8–16 wave band with a resolution of 1 km), but the spatial resolution of the GOCI satellite is higher than that of MODIS. The main uses of each band of GOCI satellite are 412 nm for yellow matter and turbidity; 443~550 nm for chlorophyll; 660, 680, and 745 nm

for fluorescence intensity; and 865 nm for aerosol. Compared with the conventional MODIS, this satellite can be used for the inversion of watercolor parameters more precisely.

Continuous high-frequency observation provides a higher possibility for the analysis of events occurring in the dynamic change of the ecosystem than general observation. At the same time, the dynamic change of the ecosystem can make more accurate accounting for such management and research. Therefore, it is clear that if there is no high-frequency sensor such as GOCI to provide hourly dynamic observation of HABs, the nature and biomass of HAB coverage are likely to be ignored or underestimated. GOCI images can obtain the hour-by-hour change characteristics of HABs in the study area and make up for the shortcomings of the traditional watercolor sensor's low time resolution, in order to provide faster and more macro data support for relevant decision-making.

Conclusion

The LMM-NDVI method was used to extract the HAB coverage of GOCI (500 m) images, and the area accuracy of the HABs extracted by GOCI was evaluated using the MODIS and high spatial resolution Landsat8 OLI image extraction results. Finally, the dynamics of HABs in Taihu Lake was analyzed with meteorological data. The results show that the NDVI threshold method is used to extract HAB pixels, then the mixed pixel decomposition results are masked, and the HAB pixel abundance after the mask is used to calculate the area of HABs, which effectively eliminates the interference of non-HAB pixels. The combination of the two can greatly improve the accuracy of HAB area extraction. When the NDVI threshold is 0.1, the overall accuracy is the highest. This method has good applicability in the different areas of the study area. The accuracy of extracting HABs from GOCI images is generally higher than that of MODIS images

with 1000-m spatial resolution. The wind speed and direction directly drive the formation, movement, and disappearance of HABs. The study shows that large-scale, high-precision, short-term spatial dynamics of HABs in Taihu Lake can be obtained using GOCI images to support decision-making and assessment of ecological hazards of HABs in Taihu Lake.

Author contribution Hongye Cao is responsible for the conceptualization, methodology, software, validation, and visualization of this article, while Ling Han is responsible for funding acquisition and supervision.

Data Availability Data sharing is not applicable to this article as no datasets were generated or analyzed during the current study.

Declaration

Ethics approval and consent to participate   Not applicable.

Consent for publication   All authors agree to have this manuscript published in this journal.

Competing interest   The authors declare no competing interests.

References

Ahn JH, Park YJ, Ryu JH, Lee B, Oh IS (2012) Development of atmospheric correction algorithm for Geostationary Ocean Color Imager (GOCI). Ocean Sci J 47:247–259

Bonansea M, Ledesma C, Rodríguez C, Pinotti L, Antunes MH (2015) Effects of atmospheric correction of Landsat imagery on lake water clarity assessment. Adv Space Res 56:2345–2355

Cannizzaro JP, Barnes BB, Hu CM, Corcoran AA, Hubbard KA, Muhlbach E, Sharp WC, Brand LE, Kelble CR (2019) Remote detection of cyanobacteria blooms in an optically shallow subtropical lagoonal estuary using MODIS data. Remote Sens Environ 231: 111227

Cao HS (2006) Study on the formation process and dominant ecological factors of cyanobacteria bloom in Taihu, Nanjing Institute of Geography & Limnology. Chinese Academy of Sciences, Nanjing

Cao RY, Chen Y, Shen MG, Chen J, Zhou J, Wang C, Yang W (2018) A simple method to improve the quality of NDVI time-series data by integrating spatiotemporal information with the Savitzky-Golay filter. Remote Sens Environ 217:244–257

Chen XR, Shang SL, Lee ZP, Qi L, Yan J, Li YH (2019) High-frequency observation of floating algae from AHI on Himawari-8. Remote Sens Environ 227:151–161

Cho M, Ramoelo A (2019) Optimal dates for assessing long-term changes in tree-cover in the semi-arid biomes of South Africa using MODIS NDVI time series (2001–2018). Int J Appl Earth Obs Geoinf 81:27–36

Chorus EI, Bartram J (1999) Toxic cyanobacteria in water: a guide to their public health consequences, monitoring and management. E & FN Spon, London, p 17

Diaz R, Rosenberg R (2008) Spreading dead zones and consequences for marine ecosystems. Science 321:926–929

Du CG, Li YM, Wang Q, Liu G, Zheng ZB, Mu M, Li Y (2017) Tempospatial dynamics of water quality and its response to river flow in estuary of Taihu Lake based on GOCI imagery. Environ Sci Pollut Res 24:28079–28101

Duan HT, Zhang SX, Zhang YZ (2008) Cyanobaeteria bloom monitoring with remote sensing in Lake Taihu. J Lake Sci 20:145–152

Duan HT, Ma RH, Hu CM (2012) Evaluation of remote sensing algorithms for cyanobacterial pigment retrievals during spring bloom formation in several lakes of East China. Remote Sens Environ 126:126–135

Foster R, Kuypers M, Vagner T, Paerl R, Musat N, Zehr J (2011) Nitrogen fixation and transfer in open ocean diatom-cyanobacterial symbioses. ISME J 5:1484–1493

Fu KZ, Moe B, Li XF, Le XC (2015) Cyanobacterial bloom dynamics in Lake Taihu. J Environ Sci (China) 32:249–251

Glibert P, Heil C, Hollander D, Revilla M, Hoare A, Alexander J, Murasko S (2004) Evidence for dissolved organic nitrogen and phosphorus uptake during a cyanobacterial bloom in Florida Bay. Mar Ecol Prog Ser 280:73–83

Gu XF, Chen XF, Yin Q, Xu H, Shao Y, Li ZW (2011) Stereoscopic remote sensing used in monitoring Enteromorpha prolifera disaster in Chinese Yellow Sea. Spectrosc Spectr Anal 31:1627–1632

Guo L (2007) Doing battle with the green monster of Taihu Lake. Science 317:1166

Higa H, Sugahara S, Salem SL, Nakamura Y, Suzuki T (2020) An estimation method for blue tide distribution in Tokyo Bay based on sulfur concentrations using Geostationary Ocean Color Imager (GOCI). Estuar Coast Shelf Sci 235:106615

Hu YK, Yu ZF, Zhou B, Li Y, Yin SJ, He XQ, Peng XX, Shum CK (2019) Tidal-driven variation of suspended sediment in Hangzhou Bay based on GOCI data. Int J Appl Earth Obs Geoinf 82:101920

Huang CC, Guo YL, Yang H, Zou J, Zhang ML, Lyu H, Zhu AX, Huang T (2015) Using remote sensing to track variation in phosphorus and its interaction with chlorophyll-a and suspended sediment. IEEE J Sel Top Appl Earth Obs Remote Sens 8:1–11

Huisman J, Matthijs HC, Visser PM (2005) Harmful cyanobacteria. Aquatic Ecology Series. Springer, Dordrecht

Jiang GJ, Ma RH, Loiselle S, Su W, Cai WX, Huang CG, Yang J, Yu W (2015) Remote sensing of particulate organic carbon dynamics in a eutrophic lake (Taihu Lake, China). Sci Total Environ 532:245–254

Kim S, Duan R, Ma GQ, Kim HY (2020) Multiresolution spatial generalized linear mixed model for integrating multi-fidelity spatial count data without common identifiers between data sources. Spat Stat 39: 100467

Kong FX, Gao G (2005) Hypothesis on cyanobacteria bloom-forming mechanism in large shallow eutrophic lakes. Acta Ecol Sin 25: 589–595

Kwon YS, Pyo JC, Kwon YH, Duan HT, Cho KH, Park Y (2020) Drone-based hyperspectral remote sensing of cyanobacteria using vertical cumulative pigment concentration in a deep reservoir. Remote Sens Environ 236:111517

Lei SH, Xu J, Li YM, Du CG, Liu G, Zheng ZB, Xu YF, Lyu H, Mu M, Miao S, Zeng S, Xu JF, Li LL (2020) An approach for retrieval of horizontal and vertical distribution of total suspended matter

concentration from GOCI data over Lake Hongze. Sci Total Environ 700:134524

Li Y, Shang SL, Zhang CY, Ma XX, Huang LW, Wu JY, Zeng YD (2005) Recognition model of algal bloom water based on the relationship between visible light and near infrared remote sensing reflectance Chin. Sci Bull 50:2555–2561

Lips I, Lips U, Leppänen JM (2003) The influence of weather conditions (temperature and wind) on cyanobacterial bloom development in the Gulf of Finland (Baltic Sea). Harmful Algae 2:29–41

Liu JG, Yang W (2012) Water sustainability for China and beyond. Science 337:649–650

Luo JH, Li XC, Ma RH, Li F, Duan HT, Hu WP, Qin BQ, Huang WJ (2016) Applying remote sensing techniques to monitoring seasonal and interannual changes of aquatic vegetation in Taihu Lake. China. Ecol Indic 60:503–513

Luo JH, Pu RL, Duan HT, Ma RH, Mao ZG, Zeng Y, Huang LS, Xiao QT (2020) Evaluating the influences of harvesting activity and eutrophication on loss of aquatic vegetations in Taihu Lake, China. Int J Appl Earth Obs Geoinf 87:102038

Lv CC, Wang ZW, Qian SM (2003) A Review of Pixel Unmixing Models. Remote Sens Inform 3:55–60

Lyit N, Genc A (2011) Constitution of random intercept and slope model (RISM) as a special case of linear mixed models (LMMs) for repeated measurements data. Appl Math Comput 218:827–831

Ma JG, Duan HT, He LY, Tiffany M, Cao ZG, Qi TC, Shen M, Biggs T, Xu XF (2020) Spatiotemporal pattern of gypsum blooms in the Salton Sea, California, during 2000-2018. Int J Appl Earth Obs Geoinf 89:102090

Ma JH, Song KS, Shao TT, Zhao Y, Wen ZD (2016) Comparison of water transparency retrieving of lakes in the mid-east part of Jilin Province based on HJ-CCD and MODIS imagery. J Lake Sci 28: 661–668

Ma RH, Kong FX, Duan HT, Zhang SX, Kong WJ, Hao JY (2008) Spatio-temporal distribution of cyanobacteria blooms based on satellite imageries in Lake Taihu, China. J Lake Sci 20:687–694

Ma RH, Kong WJ, Duan HT, Zhang SX (2009) Quantitative estimation of phycocyanin concentration using MODIS imagery during the period of cyanobacterial blooming in Taihu Lake, China. Environ Sci 29:254–260

Meng QM, Cieszewski CJ, Madden M, Borders B (2007) A linear mixed-effects model of biomass and volume of trees using Landsat ETM+ images. For Ecol Manag 244:93–101

Micheli F (1999) Eutrophication, fisheries, and consumer-resource dynamics in marine pelagic ecosystems. Science 285:1396–1398

Nazeer M, Wong MS, Nichol JE (2017) A new approach for the estimation of phytoplankton cell counts associated with algal blooms. Sci Total Environ 590-591:125–138

Noh JH, Kim W, Son SH, Ahn JH, Park YJ (2018) Remote quantification of Cochlodinium polykrikoides blooms occurring in the East Sea using geostationary ocean color imager (GOCI). Harmful Algae 73: 129–137

Norris JR, Walker JJ (2020) Solar and sensor geometry, not vegetation response, drive satellite NDVI phenology in widespread ecosystems of the western United States. Remote Sens Environ 249:112013

Oyama Y, Matsushita B, Fukushima T (2015) Distinguishing surface cyanobacterial blooms and aquatic macrophytes using Landsat/TM and ETM+ shortwave infrared bands. Remote Sens Environ 157: 35–47

Pal M, Yesankar PJ, Dwivedi A, Qureshi A (2020) Biotic control of harmful algal blooms (HABs): a brief review. J Environ Manag 268:110687

Pang JM, Liu ZQ, Wang XM, Bresch J, Ban JM, Chen D, Kim J (2018) Assimilating AOD retrievals from GOCI and VIIRS to forecast surface PM 2.5 episodes over Eastern China. Atmos Environ 179: 288–304

Qi L, Hu CM, Duan HT, Cannizzaro J, Ma RH (2014) A novel MERIS algorithm to derive cyanobacterial phycocyanin pigment concentrations in a eutrophic lake: theoretical basis and practical considerations. Remote Sens Environ 154:298–317

Qin BQ, Zhu GW, Gao G, Zhang YL, Li W, Paerl HW, Carmichael WW (2010) A drinking water crisis in Lake Taihu, China: linkage to climatic variability and lake management. Environ Manag 45:105–112

Qin BQ, Yang GJ, Ma JR, Deng JM, Li W, Wu TF, Liu LZ, Gao G, Zhu GW, Zhang YL (2016) Dynamics of variability and mechanism of harmful cyanobacteria bloom in Lake Taihu, China. Chin Sci Bull 61:759–770

Reichwaldt E, Ghadouani A (2011) Effects of rainfall patterns on toxic cyanobacterial blooms in a changing climate: between simplistic scenarios and complex dynamics. Water Res 46:1372–1393

Shi K, Zhang YL, Qin BQ, Zhou BT (2019) Remote sensing of cyanobacterial blooms in inland waters: present knowledge and future challenges. Sci Bull 64:1540–1556

Tang D, Liu DR, Tang YL, Seyler B, Deng XF, Zhan Y (2019) Comparison of GOCI and Himawari-8 aerosol optical depth for deriving full-coverage hourly PM2.5 across the Yangtze River Delta. Atmos Environ 217:116973

Vonlanthen P, Bittner D, Hudson A, Young K, Müller R, Lundsgaard-Hansen B, Roy D, Piazza S, Largiader C, Seehausen O (2012) Eutrophication causes speciation reversal in whitefish adaptive radiations. Nature 482:357–362

Wang D, Ma RH, Xue K, Loiselle S (2019a) The assessment of Landsat-8 OLI atmospheric correction Algorithms for inland waters. Remote Sens 11:169

Wang FJ, Sheng H, Su J, Min XF (2018) Refined extraction method for green tide coverage area based on GOCI data. J Geom 43:24–27

Wang JH, Yang C, He LQS, Dao GH, Du JS, Han YP, Wu GX, Wu QY, Hu HY (2019b) Meteorological factors and water quality changes of Plateau Lake Dianchi in China (1990–2015) and their joint influences on cyanobacterial blooms. Sci Total Environ 665:406–418

Wang JH, Wang YN, Dao GH, Du JS, Han YP, Hu HY (2020) Decade-long meteorological and water quality dynamics of northern Lake Dianchi and recommendations on algal bloom mitigation via key influencing factors identification. Ecol Indic 115:106425

Warren-Rhodes KA, Rhodes KL, Boyle LN, Pointing SB, Chen Y, Liu SJ, Zhuo PJ, McKay CP (2007) Cyanobacterial ecology across environmental gradients and spatial scales in China's hot and cold deserts. FEMS Microbiol Ecol 61:470–482

Wu TF, Zhu GW, Qin BQ, Ding YQ, Wu SF (2012) Prior wind field induced hydrodynamics and its influence on cyanobacterial bloom in northern bays of Lake Taihu. China. J Lake Sci 24:409–415

Wu TF, Qin BQ, Zhu GW, Luo LC, Ding YQ, Bian GY (2013) Dynamics of cyanobacteria bloom formation during short-term hydrodynamic fluctuation in a large shallow, eutrophic, and wind-exposed Lake Taihu. China. Environ Sci Pollut Res Int 20:8546–8556

Wynne TT, Stumpf RP, Tomlinson MC, Dyble J (2010) Characterizing a cyanobacterial bloom in Western Lake Erie using satellite imagery and meteorological data. Limnol Oceanogr 55:2025–2036

Xie GJ, Tang XM, Shao KQ, Hu Y, Liu H, Martin RM, Gao G (2020) Spatiotemporal patterns and environmental drivers of total and active bacterial abundances in Lake Taihu, China. Ecol Indic 114: 106335

Xu JP, Zhang B, Li F, Song KS, Wang ZM (2008) Detecting modes of cyanobacteria bloom using MODIS data in Lake Taihu. J Lake Sci 20:191–195

Xue QJ, Steinman AD, Xie LQ, Yao L, Su XM, Cao Q, Zhao YY, Cai YJ (2020) Seasonal variation and potential risk assessment of microcystins in the sediments of Lake Taihu, China. Environ Pollut 259:113884

Yang Z, Zhang M, Shi XL, Kong FX, Ma RH, Yu Y (2016) Nutrient reduction magnifies the impact of extreme weather on cyanobacterial bloom formation in large shallow Lake Taihu (China). Water Res 103:302–310

Yao XL, Zhang YL, Zhang L, Zhu GW, Qin BQ, Zhou YQ, Xue JY (2020) Emerging role of dissolved organic nitrogen in supporting algal bloom persistence in Lake Taihu, China: emphasis on internal transformations. Sci Total Environ 736:139497

Yeom JM, Ko J, Kim HO (2015) Application of GOCI-derived vegetation index profiles to estimation of paddy rice yield using the GRAMI rice model. Comput Electron Agric 118:1–8

Yeom JM, Roujean JL, Han KS, Lee KS, Kim HW (2020) Thin cloud detection over land using background surface reflectance based on the BRDF model applied to Geostationary Ocean Color Imager (GOCI) satellite data sets. Remote Sens Environ 239:111610

Yu YF, Xing LX, Pan J, Jiang LJ, Yu HL (2016) Study of high temperature targets identification and temperature retrieval experimental model in SWIR remote sensing based Landsat8. Int J Appl Earth Obs Geoinf 46:56–62

Zhou LG, Feng XZ, Wang CH, Wang DY, Xu X (2008) Monitoring cyanobacteria bloom based on MODIS data in Lake Taihu. J Lake Sci 20:203–207

Zhu YC, Cai QM (1997) The Dynamic Research of The influence of Wind Field on The Migration of Algae in Taihu Lake. J Lake Sci 9:152–158